CHAPTER 3

ON THE SOLUTION OF A THERMOELASTIC PROBLEM OF FUNCTIONALLY GRADED HOLLOW DISK UNDER STRAIN AND TEMPERATURE-RATE DEPENDENT THEORY

3.1 Introduction[1]

The present chapter is concerned with the recently introduced theory by Yu et al. (2018), who have incorporated the strain-rate term in the GL theory and formulated the modified Green-Lindsay thermoelasticity theory (MGL theory). Quintanilla (2018) has discussed the spatial behaviour of the solutions for the thermoelastic problems based on this MGL theory and established that the solution decays exponentially with time under this model.

Composite laminated plates have wide applications in various engineering applications due to the efficient use of superior material properties of individual material constituents. However, in some cases, a composite laminated structure fails because of thermal stresses at the interface of two different materials. Therefore, attempts are being made to form more accurate composites. The functionally graded materials (FGM) are the new generation of advanced composite materials that have continuously changing material properties (Birman and Byrd (2007)). These new materials are developed

[1]Content of this chapter is published in *European Journal of Mechanics A/Solids*, Vol. 80, pp. 103914, 2020.

with the purpose of designing structures that can withstand suddenly applied loads. The properties of FGM vary by a gradual change in the composition of the constituent materials through the geometry of the structure. This gradual change in material properties of FGMs makes them appropriate for the application at abruptly high applied load. Moreover, the smooth variation of properties within FGMs results in lower stress concentration, intensity factors, higher fracture toughness and improved residual stress distribution as compared to the traditional laminated composites. Therefore, FGMs have wide applications as thermal shields, wear-resistant linings, heat exchanger tubes, heat engine components and even prostheses (see Birman and Byrd (2007) and Bagri and Eslami (2007a) and references therein). The analysis of FGM structures has therefore drawn the serious attention of researchers to analyze the response of FGM under different applied mechanical and thermal loads. Several researchers have worked on FGM to optimize its potential and developed different modeling strategies depending on their responses to various thermomechanical loads (see articles by Fukui (1991); Obata and Noda (1995); Markworth et al. (1995); Zimmerman and Lutz (1999) and refs. therein). The article reported by Swaminathan et al. (2015) is worth to be mentioned here for a state of the art review of FGM plates for stress, vibration and bulking analysis. Dai et al. (2016) have also reviewed the works on FGM cylindrical structures. Swaminathan and Sangeetha (2017) have explored the various modeling techniques and solution methods for the thermal analysis of FGMs.

In the previous chapter, a complete finite element method is successfully implemented for the solution of a coupled thermoelastic problem that investigated the temperature-rate dependent thermoelasticity (TRD) theory. The complete FEM is shown to be used as an alternative method to the trans-FEM method to solve such problems. However, it is worth to discuss more about the efficiency of this method over other existing methods. In chapter 2, the predictions of the TRD (GL) theory have been compared with LS thermoelasticity theory and the variations in field variables due to temperature-

rate terms in governing equations have been discussed. Some researchers, including Chandrasekharaiah and Srikantiah (1987), Dhaliwal and Rokne (Dhaliwal and Rokne, 1989) and Ignaczak and Mrowka-Matejewska (1990), have investigated that TRD theory exhibits the discontinuity in the displacement field which suggests that one part of matter penetrates into the other, which disobeys the continuum hypothesis. In order to remove this unrealistic behaviour, Yu et al. (2018) have suggested to incorporate the effect of strain-rate along with the temperature-rate term in the constitutive relations for modeling the coupled thermoelasticity theory. This new thermoelasticity theory is yet to get attention and deserves to be investigated further.

The present chapter is therefore aimed at investigating this modified Green-Lindsay thermoelasticity theory involving additional strain-rate effects. Here a problem involving coupled thermomechanical interactions inside a functionally graded hollow disk is considered where thermal shocks are applied at both its stress-free inner and outer boundaries. The material properties of the disk are assumed to be non-homogeneous and change along the radial direction according to a volume fraction rule with a power of non-homogeneity index term. The problem is formulated by considering the basic governing equations of GL and modified GL thermoelasticity theories in a unified form to derive a linear system of coupled partial differential equations with variable coefficients. There are two major objectives of this chapter, first is to show the efficiency of the complete finite element method over the other existing FEM techniques for solving coupled dynamical problems, and the second is to investigate the newly proposed thermoelasticity theory and analyze the effects of the strain-rate term for a thermoelastic problem. The system of equations is solved by applying Galerkin's approach of FEM for the space domain and derive the time differential system of equations. In order to solve the time differential system of equations, complete Galerkin's type FE approach is applied. For the validation of results, the time differential system is also solved by employing the Newmark time integration approach (see article by Rincon et al. (2005)).

The results obtained from these different approaches are compared, and it is observed that the solution obtained by complete Galerkin's approach of FEM perfectly matches with the corresponding solution obtained from the Newmark time integration scheme. Further, a comparison is also made for the present solution with the corresponding solution by the trans-FEM method. The CPU time taken by the first two methods are compared with the CPU time taken by the trans-finite element method using bar plots, and it reveals the efficiency of the present method over the trans-FEM method. The variation of different physical field variables with space and time is discussed for various values of the non-homogeneity index by highlighting the difference in the results under the GL model and modified GL model.

3.2 Basic Governing Equations and Problem Formulation

The present study is attempted to investigate the temperature-rate dependent (GL) thermoelasticity theory (Green and Lindsay (1972)) and strain temperature-rate dependent (modified GL (MGL) theory Yu et al. (2018)) theory. Therefore we derive the unified basic governing equations in the contexts of these two theories for isotropic media. Firstly, the governing equations for MGL theory are taken as follows:

The equation of motion in absence of external body force:

$$\sigma_{ij,j} = \rho \ddot{u}_i. \tag{3.2.1}$$

The stress-strain-temperature relation:

$$\sigma_{ij} = \lambda(e_{kk} + t_1 \dot{e}_{kk})\delta_{ij} + 2\mu(e_{ij} + t_1 \dot{e}_{ij}) - \beta\delta_{ij}(\theta + t_1 \dot{\theta}). \tag{3.2.2}$$

The entropy equation without heat source:

$$\rho T_0 S = \beta(e_{kk} + t_2 \dot{e}_{kk}) + \rho T_0 c_E(\theta + t_2 \dot{\theta}). \tag{3.2.3}$$

The heat conduction law:

$$q_i = -K\theta_{,i}. \tag{3.2.4}$$

The energy equation:

$$\rho T_0 \dot{S} = -q_{i,i}. \tag{3.2.5}$$

In case of GL model, the Eqs. (3.2.2) and (3.2.3) will be replaced by the following equations:

$$\sigma_{ij} = \lambda e_{kk}\delta_{ij} + 2\mu e_{ij} - \beta\delta_{ij}(\theta + t_1\dot{\theta}), \tag{3.2.6}$$

$$\rho T_0 S = \beta e_{kk} + \rho T_0 c_E(\theta + t_2\dot{\theta}). \tag{3.2.7}$$

Hence, Eqs. (3.2.1-3.2.5) constitute the basic equations for MGL theory and Eqs. (3.2.1,3.2.4-3.2.6), and (3.2.7) constitute the corresponding equations in the context of GL theory.

Now, from Eqs (3.2.3-3.2.5), we derive the heat conduction equation under MGL theory as

$$\left(K\theta_{,i}\right)_{,i} = \beta(\dot{e}_{kk} + t_2\ddot{e}_{kk}) + \rho T_0 c_E(\dot{\theta} + t_2\ddot{\theta}). \tag{3.2.8}$$

Similarly, Eqs. (3.2.4-3.2.5,3.2.7) yield the heat conduction equation in the context of GL model as

$$\left(K\theta_{,i}\right)_{,i} = \beta\dot{e}_{kk} + \rho T_0 c_E(\dot{\theta} + t_2\ddot{\theta}). \tag{3.2.9}$$

In view of Eqs. (3.2.2,3.2.6) and Eqs. (3.2.8-3.2.9), the unified form of stress-strain-temperature relation and heat conduction equations for GL and MGL models can be written in the following forms:

$$\sigma_{ij} = \lambda(e_{kk} + pt_1\dot{e}_{kk})\delta_{ij} + 2\mu(e_{ij} + pt_1\dot{e}_{ij}) - \beta\delta_{ij}(\theta + t_1\dot{\theta}), \tag{3.2.10}$$

$$\left(K\theta_{,i}\right)_{,i} = \beta(\dot{e}_{kk} + pt_2\ddot{e}_{kk}) + \rho T_0 c_E(\dot{\theta} + t_2\ddot{\theta}), \tag{3.2.11}$$

where p is the parameter used to write the unified equations of GL and MGL theory. The Eqs. (3.2.1,3.2.10-3.2.11) represent the equations for GL and MGL models in a

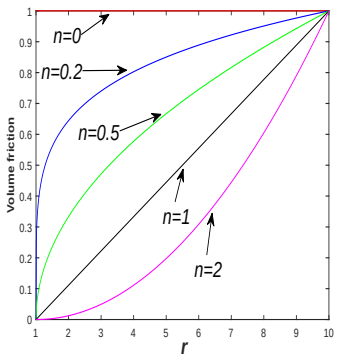

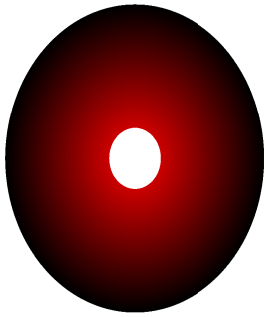

(a) (b)

Figure 3.2.1: (a) Variation on volume fraction for different n, (b) Distribution of metallic (shown in red color) and ceramic (shown in black color) property inside the hollow disk for $n = 1$

unified form, and these equations can be obtained under two different theories by setting the values of parameter p as follows:

Case I: $p = 0$ (GL theory)

Case II: $p = 1$ (MGL theory).

Also, by combining the Eqs. (3.2.1) and (3.2.10), the unified form of equation of motion can be given as

$$\Big[\lambda(e_{kk} + pt_1\dot{e}_{kk})\delta_{ij} + 2\mu(e_{ij} + pt_1\dot{e}_{ij}) - \beta(\theta + t_1\dot{\theta})\Big]_{,j} - \rho\ddot{u}_i = 0. \tag{3.2.12}$$

Statement of the Problem:

A coupled thermomechanical plane stress problem of a functionally graded hollow disk is considered, which is composed of two different materials, metallic and ceramic (see Fig. 3.2.1(a,b)). It is assumed that the properties of the material are varying radially and follow a volume fraction rule with the power of a non-homogeneity index term. Based on this assumption, the formula for effective material properties can be written as

$$M = \left(\frac{r-a}{b-a}\right)^n (M_m - M_c) + M_c. \tag{3.2.13}$$

where M stands for any material property, where the subscripted m and c are denoting the metallic and ceramic nature. a and b are the inner and outer radius of the disk, r is the radial position of any point inside the disk. n is the non-homogeneity index, and with variation in the values of n, we can obtain the different profiles of material parameters. For $n = 0$ the material is metallic, and it will be ceramic if $n \to \infty$.

It is assumed that all the material properties, except relaxation parameters used in Eqs. (3.2.1-3.2.12) are not constant but dependent on radial coordinate r and satisfy the relation (3.2.13). The inner and outer boundaries of the disk are taken at the same initial reference temperature T_0 and thermal shocks are applied at its inner and outer boundaries. Now, the Eqs. (3.2.10-3.2.12) with the assumption of the plane stress condition, will reduce to the forms:

$$\sigma_{rr} = \left(1 + pt_1\frac{\partial}{\partial t}\right)\left[2\mu\frac{\partial u}{\partial r} + \bar{\lambda}\left(\frac{\partial u}{\partial r} + \frac{u}{r}\right)\right] - \bar{\beta}\left(1 + t_1\frac{\partial}{\partial t}\right)\theta, \tag{3.2.14}$$

$$\sigma_{\phi\phi} = \left(1 + pt_1\frac{\partial}{\partial t}\right)\left[2\mu\frac{u}{r} + \bar{\lambda}\left(\frac{\partial u}{\partial r} + \frac{u}{r}\right)\right] - \bar{\beta}\left(1 + pt_1\frac{\partial}{\partial t}\right)\theta, \tag{3.2.15}$$

$$K\left(\frac{\partial^2\theta}{\partial r^2} + \frac{1}{r}\frac{\partial\theta}{\partial r}\right) + \frac{\partial K}{\partial r}\frac{\partial\theta}{\partial r} - \rho c_E\left(1 + t_2\frac{\partial}{\partial t}\right)\frac{\partial\theta}{\partial t} - \bar{\beta}T_0\left(1 + pt_2\frac{\partial}{\partial t}\right)\frac{\partial}{\partial t}\left(\frac{\partial u}{\partial r} + \frac{u}{r}\right) = 0, \tag{3.2.16}$$

$$\left(1 + pt_1\frac{\partial}{\partial t}\right)\left[(\bar{\lambda} + 2\mu)\left(\frac{\partial^2 u}{\partial r} + \frac{1}{r}\frac{\partial u}{\partial r} - \frac{u}{r^2}\right) + \frac{\partial u}{\partial r}\frac{\partial(\bar{\lambda} + 2\mu)}{\partial r} + \frac{u}{r}\frac{\partial\bar{\lambda}}{\partial r}\right] - \left(1 + t_1\frac{\partial}{\partial t}\right)\left[\bar{\beta}\frac{\partial\theta}{\partial r} + \theta\frac{\partial\bar{\beta}}{\partial r}\right] - \rho\frac{\partial^2 u}{\partial r^2} = 0. \tag{3.2.17}$$

where $\bar{\lambda} = \frac{2\mu}{\lambda+2\mu}\lambda$ and $\bar{\beta} = \frac{2\mu}{\lambda+2\mu}\beta$.

In addition to the basic equations given by Eqs. (3.2.14-3.2.17), the homogeneous initial conditions together with the boundary conditions are considered as

$$\begin{aligned} \theta &= 1 - e^{-10^4 t},\ \sigma_{rr} = 0,\ \text{at}\, r = a \\ \theta &= 1 - e^{-10^4 t},\ \sigma_{rr} = 0,\ \text{at}\, r = b \end{aligned}, \tag{3.2.18}$$

Now, the following non-dimensional transformations of the variables are used:

$r' = c_1 n_0 r,\ \theta' = \frac{\theta}{T_0},\ (t', t_1', t_2') = c_1^2 n_0 (t, t_1, t_2),\ u' = \frac{c_1 n_0 (\bar{\lambda}_m + 2\mu_m)}{\bar{\beta}_m T_0} u,\ (\sigma_{rr}', \sigma_{\phi\phi}') = \frac{(\sigma_{rr}, \sigma_{\phi\phi})}{\beta_m T_0}$,
where $c_1^2 = \frac{(\bar{\lambda}_m + 2\mu_m)}{\rho_m}$, $n_0 = \frac{\rho_m c_E}{K_m}$.

By substituting the above non-dimensional variables and parameters, dimensionless form of Eqs. (3.2.14-3.2.17) are obtained as

$$\sigma_{rr} = \left(1 + pt_1 \frac{\partial}{\partial t}\right) \left[\frac{2\mu}{(\bar{\lambda}_m + 2\mu_m)} \frac{\partial u}{\partial r} + \frac{\bar{\lambda}}{(\bar{\lambda}_m + 2\mu_m)} \left(\frac{\partial u}{\partial r} + \frac{u}{r}\right)\right] - \frac{\bar{\beta}}{\bar{\beta}_m} \left(1 + t_1 \frac{\partial}{\partial t}\right) \theta, \tag{3.2.19}$$

$$\sigma_{\phi\phi} = \left(1 + pt_1 \frac{\partial}{\partial t}\right) \left[\frac{2\mu}{(\bar{\lambda}_m + 2\mu_m)} \frac{u}{r} + \frac{\bar{\lambda}}{(\bar{\lambda}_m + 2\mu_m)} \left(\frac{\partial u}{\partial r} + \frac{u}{r}\right)\right] - \frac{\bar{\beta}}{\bar{\beta}_m} \left(1 + t_1 \frac{\partial}{\partial t}\right) \theta, \tag{3.2.20}$$

$$\frac{K}{K_m} \left(\frac{\partial^2 \theta}{\partial r^2} + \frac{1}{r} \frac{\partial \theta}{\partial r}\right) + \frac{1}{K_m} \frac{\partial K}{\partial r} \frac{\partial \theta}{\partial r} - \frac{\rho c_E}{\rho_m (c_E)_m} \left(1 + t_2 \frac{\partial}{\partial t}\right) \frac{\partial \theta}{\partial t} - \varepsilon \frac{\bar{\beta}}{\bar{\beta}_m} \left(1 + pt_2 \frac{\partial}{\partial t}\right) \frac{\partial}{\partial t} \left(\frac{\partial u}{\partial r} + \frac{u}{r}\right) = 0, \tag{3.2.21}$$

$$\left(1 + pt_1 \frac{\partial}{\partial t}\right) \left[(\bar{\lambda} + 2\mu) \left(\frac{\partial^2 u}{\partial r} + \frac{1}{r} \frac{\partial u}{\partial r} - \frac{u}{r^2}\right) + \frac{\partial u}{\partial r} \frac{\partial (\bar{\lambda} + 2\mu)}{\partial r} + \frac{u}{r} \frac{\partial \bar{\lambda}}{\partial r}\right] - \left(1 + t_1 \frac{\partial}{\partial t}\right) \frac{(\bar{\lambda}_m + 2\mu_m)}{\bar{\beta}_m} \left[\bar{\beta} \frac{\partial \theta}{\partial r} + \theta \frac{\partial \bar{\beta}}{\partial r}\right] - \rho c_1^2 \frac{\partial^2 u}{\partial r^2} = 0, \tag{3.2.22}$$

where $\varepsilon = \frac{\bar{\beta}_m^2 T_0}{(\bar{\lambda}_m + 2\mu_m) \rho_m (c_E)_m}$. In the above equations, we omitted the primes for simplicity.

3.3 Finite Element Formulation

Now, in order to solve the problem as described in the previous section, firstly, the generalized formulation of finite element equations for Eqs. (3.2.21-3.2.22) in the space domain is derived. For this the radial domain $[a, b]$ is discretized in h sub-intervals ($[r_i, r_{i+1}],\ i = 1, 2...h$) of equal length l. Therefore, each sub-interval will denote a separate element of the domain. For any element (e), we approximate the nodal functions u and θ as

$$\left.\begin{aligned} u^{(e)} &= U_i(t)N_1 + U_{i+1}(t)N_2 \\ \theta^{(e)} &= \Theta_i(t)N_1 + \Theta_{i+1}(t)N_2 \end{aligned}\right\}, \tag{3.3.1}$$

where U_i, Θ_i and U_{i+1}, Θ_{i+1} are the values of nodal functions u and θ at nodal points r_i and r_{i+1}, respectively. N_1 and N_2 are taken as the Lagrangian shape functions. Now, applying the Galerkin's approach of FEM over any base element (e) of volume V^e and taking N_k as weight function, we have

$$\begin{aligned} \int_{V^e} N_k \Bigg[\frac{K}{K_m}\left(\frac{\partial^2}{\partial r^2} + \frac{1}{r}\frac{\partial}{\partial r}\right)\theta^{(e)} + \frac{1}{K_m}\frac{\partial K}{\partial r}\frac{\partial \theta^{(e)}}{\partial r} - \frac{\rho c_E}{\rho_m (c_E)_m}\left(1 + t_2\frac{\partial}{\partial t}\right)\frac{\partial \theta^{(e)}}{\partial t} \\ -\varepsilon\frac{\bar{\beta}}{\bar{\beta}_m}\left(1 + pt_2\frac{\partial}{\partial t}\right)\frac{\partial}{\partial t}\left(\frac{\partial}{\partial r} + \frac{1}{r}\right)u^{(e)}\Bigg] dV = 0, \end{aligned} \tag{3.3.2}$$

$$\begin{aligned} \int_{V^e} N_k \Bigg[\left(1 + pt_1\frac{\partial}{\partial t}\right)\left[(\bar{\lambda} + 2\mu)\left(\frac{\partial^2}{\partial r^2} + \frac{1}{r}\frac{\partial}{\partial r} - \frac{1}{r^2}\right) + \frac{\partial}{\partial r}\frac{\partial(\bar{\lambda} + 2\mu)}{\partial r} + \frac{1}{r}\frac{\partial \bar{\lambda}}{\partial r}\right]u^{(e)} \\ - \left(1 + t_1\frac{\partial}{\partial t}\right)\frac{(\bar{\lambda}_m + 2\mu_m)}{\bar{\beta}_m}\left[\bar{\beta}\frac{\partial}{\partial r} + \frac{\partial \bar{\beta}}{\partial r}\right]\theta^{(e)} - \rho c_1^2\frac{\partial^2 u^{(e)}}{\partial r^2}\Bigg] dV = 0. \end{aligned} \tag{3.3.3}$$

Further, for the radial disk, the infinitesimal volume element $dV = rdr$ is assumed and hence, deriving the weak form of Eqs. (3.3.2-3.3.3) with the assumption of nodal functions as Eq. (3.3.1), the simplified equations are obtained as

$$\begin{aligned} \int_{r_i}^{r_{i+1}} r\frac{K}{K_m}\left(\frac{\partial N_k}{\partial r}\frac{\partial N_1}{\partial r}\Theta_i + \frac{\partial N_k}{\partial r}\frac{\partial N_2}{\partial r}\Theta_{i+1}\right)dr + \\ \int_{r_i}^{r_{i+1}} r\frac{\rho c_E}{\rho_m (c_E)_m}\left(N_k N_1\dot{\Theta}_i + N_k N_2\dot{\Theta}_{i+1}\right)dr + \\ t_0\int_{r_i}^{r_{i+1}} r\frac{\rho c_E}{\rho_m (c_E)_m}\left(N_k N_1\ddot{\Theta}_i + N_k N_2\ddot{\Theta}_{i+1}\right)dr \\ +\varepsilon\int_{r_i}^{r_{i+1}} r\frac{\bar{\beta}}{\bar{\beta}_m}N_k\left[\left(\frac{\partial N_1}{\partial r} + \frac{N_2}{r}\right)\dot{U}_i + \left(\frac{\partial N_2}{\partial r} + \frac{N_2}{r}\right)\dot{U}_{i+1}\right]dr + \\ t_1\varepsilon\int_{r_i}^{r_{i+1}} r\frac{\bar{\beta}}{\bar{\beta}_m}N_k\left[\left(\frac{\partial N_1}{\partial r} + \frac{N_2}{r}\right)\ddot{U}_i + \left(\frac{\partial N_2}{\partial r} + \frac{N_2}{r}\right)\ddot{U}_{i+1}\right]dr = rN_k\frac{K}{K_m}\frac{\partial \theta}{\partial r}\Bigg|_{r_i}^{r_{i+1}}, \end{aligned} \tag{3.3.4}$$

$$\begin{aligned}
&\int_{r_i}^{r_{i+1}} \left(\left[(\bar{\lambda}+2\mu) \left(r\frac{\partial N_k}{\partial r}\frac{\partial N_1}{\partial r} + \frac{N_k N_1}{r} \right) + r\frac{\partial \bar{\lambda}}{\partial r} N_k N_1 \right] U_i \right. \\
&\left. + \left[(\bar{\lambda}+2\mu) \left(r\frac{\partial N_k}{\partial r}\frac{\partial N_2}{\partial r} + \frac{N_k N_2}{r} \right) + r\frac{\partial \bar{\lambda}}{\partial r} N_k N_2 \right] U_{i+1} \right) dr \\
&\int_{r_i}^{r_{i+1}} pt_1 \left(\left[(\bar{\lambda}+2\mu) \left(r\frac{\partial N_k}{\partial r}\frac{\partial N_1}{\partial r} + \frac{N_k N_1}{r} \right) + r\frac{\partial \bar{\lambda}}{\partial r} N_k N_1 \right] \dot{U}_i \right. \\
&\left. + \left[(\bar{\lambda}+2\mu) \left(r\frac{\partial N_k}{\partial r}\frac{\partial N_2}{\partial r} + \frac{N_k N_2}{r} \right) + r\frac{\partial \bar{\lambda}}{\partial r} N_k N_2 \right] \dot{U}_{i+1} \right) dr + \\
&\frac{\bar{\lambda}+2\mu}{\bar{\beta}_m} \int_{r_i}^{r_{i+1}} \left[rN_k \left(\bar{\beta}\frac{\partial N_1}{\partial r} + N_1\frac{\partial \bar{\beta}}{\partial r} \right) \Theta_i + rN_k \left(\bar{\beta}\frac{\partial N_1}{\partial r} + N_1\frac{\partial \bar{\beta}}{\partial r} \right) \Theta_{i+1} \right] dr \\
&+ t_1 \frac{\bar{\lambda}+2\mu}{\bar{\beta}_m} \int_{r_i}^{r_{i+1}} \left[rN_k \left(\bar{\beta}\frac{\partial N_1}{\partial r} + N_1\frac{\partial \bar{\beta}}{\partial r} \right) \Theta_i + rN_k \left(\bar{\beta}\frac{\partial N_1}{\partial r} + N_1\frac{\partial \bar{\beta}}{\partial r} \right) \Theta_{i+1} \right] dr \\
&+ \int_{r_i}^{r_{i+1}} rN_k \rho c_1^2 (N_1 \ddot{U}_i + N_2 \ddot{U}_{i+1}) dr = N_k r \left(1 + pt_1 \frac{\partial}{\partial t} \right) \frac{K}{K_m} \frac{\partial u}{\partial r} \Big|_{r_i}^{r_{i+1}}.
\end{aligned} \tag{3.3.5}$$

Now, in view of Eqs. (3.3.4-3.3.5) and taking $k = 1, 2$, the element matrix is found as

$$C^{(e)}\ddot{X} + B^{(e)}\dot{X} + +A^{(e)}X = F^{(e)}. \tag{3.3.6}$$

where $A^{(e)} = \begin{bmatrix} A^{11} & A^{12} \\ A^{21} & A^{22} \end{bmatrix}^{(e)}$, $B^{(e)} = \begin{bmatrix} B^{11} & B^{12} \\ B^{21} & B^{22} \end{bmatrix}^{(e)}$, $C^{(e)} = \begin{bmatrix} C^{11} & C^{12} \\ C^{21} & C^{22} \end{bmatrix}^{(e)}$,

$F^{(e)} = \begin{bmatrix} F_U \\ F_\Theta \end{bmatrix}^{(e)}$ and $X = \begin{bmatrix} U \\ \Theta \end{bmatrix}^{(e)}$ and

$A_{kj}^{11} = \int_{r_i}^{r_{i+1}} \left[(\bar{\lambda}+2\mu) \left(r\frac{\partial N_k}{\partial r}\frac{\partial N_j}{\partial r} + \frac{N_k N_j}{r} \right) + r\frac{\partial \bar{\lambda}}{\partial r} N_k N_j \right] dr,$

$B_{kj}^{11} = pt_1 \int_{r_i}^{r_{i+1}} \left[(\bar{\lambda}+2\mu) \left(r\frac{\partial N_k}{\partial r}\frac{\partial N_j}{\partial r} + \frac{N_k N_j}{r} \right) + r\frac{\partial \bar{\lambda}}{\partial r} N_k N_j \right] dr \ , C_{kj}^{11} = 0$

$A_{kj}^{12} = \frac{\bar{\lambda}+2\mu}{\bar{\beta}_m} \int_{r_i}^{r_{i+1}} \left[rN_k \left(\bar{\beta}\frac{\partial N_j}{\partial r} + N_j\frac{\partial \bar{\beta}}{\partial r} \right) \right] dr,$

$B_{kj}^{12} = t_1 \frac{\bar{\lambda}+2\mu}{\bar{\beta}_m} \int_{r_i}^{r_{i+1}} \left[rN_k \left(\bar{\beta}\frac{\partial N_j}{\partial r} + N_j\frac{\partial \bar{\beta}}{\partial r} \right) \right] dr, \ C_{kj}^{12} = 0$

$A_{kj}^{21} = 0, \ B_{kj}^{21} = \varepsilon \int_{r_i}^{r_{i+1}} r\frac{\bar{\beta}}{\bar{\beta}_m} N_k \left[\left(\frac{\partial N_j}{\partial r} + \frac{N_j}{r} \right) \right] dr,$

$C_{kj}^{21} = \varepsilon \int_{r_i}^{r_{i+1}} r\frac{\bar{\beta}}{\bar{\beta}_m} N_k \left[\left(\frac{\partial N_j}{\partial r} + \frac{N_j}{r} \right) \right] dr$

$A_{kj}^{22} = \int_{r_i}^{r_{i+1}} r\frac{K}{K_m} \left(\frac{\partial N_k}{\partial r}\frac{\partial N_j}{\partial r} \right) dr, \ B_{kj}^{22} = \int_{r_i}^{r_{i+1}} r\frac{\rho c_E}{\rho_m (c_E)_m} (N_k N_j) \, dr,$

$C_{kj}^{22} = t_0 \int_{r_i}^{r_{i+1}} r\frac{\rho c_E}{\rho_m (c_E)_m} (N_k N_j) \, dr.$

$$U = \begin{bmatrix} U_i \\ U_{i+1} \end{bmatrix}, \Theta = \begin{bmatrix} \Theta_i \\ \Theta_{i+1} \end{bmatrix}, F_U = \begin{bmatrix} -N_k r(1+pt_1\frac{\partial}{\partial t})\frac{K}{K_m}\frac{\partial u}{\partial r}\Big|_{r_i} \\ N_k r(1+pt_1\frac{\partial}{\partial t})\frac{K}{K_m}\frac{\partial u}{\partial r}\Big|_{r_{i+1}} \end{bmatrix} \text{ and}$$

$$F_\Theta = \begin{bmatrix} -rN_k\frac{K}{K_m}\frac{\partial\theta}{\partial r}\Big|_{r_i} \\ rN_k\frac{K}{K_m}\frac{\partial\theta}{\partial r}\Big|_{r_{i+1}} \end{bmatrix}.$$

Next, to obtain the global matrix of finite element, the element equation (Eq. (3.3.6)) is assembled for all elements under the consideration of boundary conditions (3.2.18), and global finite element equation is obtained in time differential form for the whole space domain as

$$\bar{C}\ddot{\chi} + \bar{B}\dot{\chi} + \bar{A}\chi = \bar{F}. \tag{3.3.7}$$

where $\bar{C}$, $\bar{B}$ and $\bar{A}$ are the global matrices corresponding to element matrices $C^{(e)}$, $B^{(e)}$ and $A^{(e)}$, respectively, and

$$\chi = \begin{bmatrix} U_1 & U_2 & \Theta_2 & U_3 & U_4 & \Theta_3 & ... & U_{h-1} & \Theta_{h-1} & U_h \end{bmatrix}^T.$$

3.4 Formulation for the Time Domain

3.4.1 I: Galerkin type FEM Formulation

In this subsection, an alternative approach (see refs. Stasa (Stasa, 1985); Balla (Balla, 1989)) based on Galerkin's type finite element is derived to solve the system of differential Eq. (3.3.7). For this FEM approach, the time domain $[0, T^*]$ is divided into a finite number of sub-intervals of equal length $2\Delta t$ and for each sub-interval $[t_{i-1}, t_{i+1}]$, three nodal values χ_{i-1}, χ_i, χ_{i+1} are considered at nodal points t_{i-1}, t_i, t_{i+1}. Then, for the interval $[t_{i-1}, t_{i+1}]$, we take the approximation of χ as

$$\chi = M_{i-1}\chi_{i-1} + M_i\chi_i + M_{i+1}\chi_{i+1}, \tag{3.4.1}$$

where $M_{i-1} = -s(1-s)/2$, $M_i = (1+s)(1-s)$, $M_{i+1} = s(1+s)/2$, are taken as the quadratic shape functions and $s = \frac{t-t_i}{t_{i+1}-t_i}$, for $t_{i-1} < t < t_{i+1}$.

Similarly, it can also be assumed that

$$F = M_{i-1}F_{i-1} + M_iF_i + M_{i+1}F_{i+1}. \tag{3.4.2}$$

Next, the Galerkin's approach of FEM is applied on Eq. (3.3.7) for any element, $[t_{i-1}, t_{i+1}]$ and consider infinitesimal time dt with shape function M_{i+1} (see ref. Stasa (1985)). Then, Eq. (3.3.7) yields

$$\int_{t_{i-1}}^{t_{i+1}} M_{i+1}\{\bar{A}\chi + \bar{B}\dot{\chi} + \bar{C}\ddot{\chi} - \bar{F}\}dt = 0. \tag{3.4.3}$$

Therefore, by substituting the relations (3.4.1-3.4.2) into Eq. (3.4.3), and deriving the weak form of Eq. (3.4.3), we find an explicit iterative scheme as

$$\Upsilon_{i+1}\chi_{i+1} = \Upsilon_i\chi_i + \Upsilon_{i-1}\chi_{i-1} + F^*, \tag{3.4.4}$$

where

$$\left.\begin{aligned} \Upsilon_{i+1} &= \bar{C} + 1.5\Delta t\bar{B} + 0.8(\Delta t)^2\bar{A} \\ \Upsilon_i &= 2\bar{C} + 2\Delta t\bar{B} - 0.4(\Delta t)^2\bar{A} \\ \Upsilon_{i-1} &= \bar{C} - 0.5\Delta t\bar{B} + 0.2(\Delta t)^2\bar{A} \\ F^* &= (\Delta t)^2[0.8F_{i-1} + 0.4F_i - 0.2F_{i-1}] \end{aligned}\right\}. \tag{3.4.5}$$

Hence, using Eq. (3.4.4) along with Eq. (3.4.5), the solution of the present thermoelastic problem can be obtained for any time steps if the values of χ_i are known for $i = 0, 1$. For $i = 0$, χ_0 is known from the initial conditions and to determine χ_1, we use the Crank-Nicholson iterative scheme, which can be given as

$$\left[\frac{2}{\Delta t}\bar{C} + \bar{B} + \frac{\Delta t}{2}\bar{A}\right]\chi_1 = \left[\frac{2}{\Delta t}\bar{C} + \bar{B} - \frac{\Delta t}{2}\bar{A}\right]\chi_0 + 2\bar{A}\dot{\chi}_0 + \frac{\Delta t}{2}\left[F_0 + F_1\right]. \tag{3.4.6}$$

3.4.2 II: Newmark Scheme

Now, for the validation of the results as obtained by above method, further the Newmark time integration method (see Rincon et al. (2005), Hasanpour and Mirzaei (2018)) is employed. For this, the time domain $[0, T^*]$ is partitioned into m sub-intervals s.t. $t_i = i\Delta t_1$ for $i = 0, 1, ...m$. Now, if it is assumed that $\chi(t_i) = \chi_i$, $\dot{\chi}(t_i) = \gamma_i$ and $\ddot{\chi}(t_i) = Z_i$, then from the homogeneous initial conditions, we have $\chi_0 = 0$ and $\gamma_0 = 0$.

Therefore, by following Hasanpour and Mirzaei (2018), the approximations for χ_{i+1} and γ_{i+1} is given as

$$\chi_{i+1} = \chi_i + \Delta t_1 \gamma_i + \frac{(\Delta t_1)^2}{2}[(1-2\omega)Z_i + 2\omega Z_{i+1}],$$

and

$$\gamma_{i+1} = \gamma_i + \Delta t_1[(1-\omega_1)Z_i + \omega_1 Z_{i+1}].$$

where ω and ω_1 are the parameters determining the stability and accuracy of the method. Now, we adopt the following Newmark predictor-corrector scheme

$$\chi_{i+1}^{(p)} = \chi_i + \Delta t_1 \gamma_i^{(p)} + \frac{(\Delta t_1)^2}{2}(1-2\omega)Z_i, \tag{3.4.7}$$

$$\gamma_{i+1}^{(p)} = \gamma_i + (1-\omega_1)\Delta t_1 Z_i. \tag{3.4.8}$$

The Eqs. (3.4.7-3.4.8) can be modified as

$$\chi_{i+1} = \chi_{i+1}^{(p)} + \omega(\Delta t_1)^2 Z_{i+1}, \tag{3.4.9}$$

$$\gamma_{i+1} = \gamma_{i+1}^{(p)} + \omega_1 \Delta t_1 Z_{i+1}. \tag{3.4.10}$$

For the first step, we calculate Z_0 from

$$\bar{C}Z_0 = F(0) - \bar{B}\gamma_0 - \bar{A}\chi_0, \tag{3.4.11}$$

and for the further iterations, we use the relation

$$(\bar{C} + \omega_1 \Delta t_1 \bar{B} + \omega(\Delta t_1)^2 \bar{A})Z_{i+1} = F(t_{i+1}) - \bar{B}\gamma_{i+1}^{(p)} - \bar{A}\chi_{i+1}^{(p)}. \tag{3.4.12}$$

Following this predictor-corrector scheme given by Eqs. (3.4.9-3.4.12), the solution for each time step is derived by taking a suitable choice of constants ω and ω_1. Newmark method can be implicit or explicit and conditionally or unconditionally stable based on different values of these constants (Hasanpour and Mirzaei (2018)).

3.5 Numerical Results and Discussion

Now, the MATLAB programs are developed for both approaches (Newmark and complete FEM), as discussed in the previous section, to obtain the numerical results of the present problem. Here, the objective is to analyze the effects of the non-homogeneity parameter and space-time variation of the field variables (displacement, temperature, radial stress and circumferential stress) inside the hollow disk under the MGL theory and GL theory. The hollow disk is initially assumed at the reference temperature $T_0 = 293\,K$, subjected to homogeneous initial conditions and boundary conditions (3.2.18). The functionally graded material is taken to be a composite of Titanium metal and Zirconia ceramic material and following the rule given by Eq. (3.2.13). For the Newmark method the parameters ω, ω_1 are taken as $\omega = 1/4$ and $\omega_1 = 1/2$ (see Hasanpour and Mirzaei (2018)). The numerical values of the parameters are taken as follows (Bahtui and Eslami (2007)):

For Titanium:

$E_m = 66.2$ GPa, $\nu_m = 0.321$, $(\alpha_t)_m = 10.3 \times 10^{-6}\mathrm{K}^{-1}$, $(c_E)_m = 808.3$ J kg^{-1}K^{-1},

ρ_m=4410 kg m^{-3}, K_m=18.1 K^{-1} s^{-1}.

For zirconia:

$E_c = 117$ GPa, $\nu_c = 0.333$, $(\alpha_t)_c = 7.11 \times 10^{-6}\mathrm{K}^{-1}$, $(c_E)_c = 615.6$ J kg^{-1}K^{-1},

ρ_c=5600 kg m^{-3}, K_c=2.036 K^{-1} s^{-1}.

The Lame's parameters are calculated as $\lambda = \frac{E\nu}{(1+\nu)(1-2\nu)}$ and $\mu = \frac{E}{2(1+\nu)}$. The dimensionless values of a and b are assumed as 1 and 5, respectively, and we consider $T^* = 1$. For both space and time, the general formulation of global finite element equation is derived. For showing numerical results, both space and time domain are divided into 100 sub-intervals.

The relaxation times are also the material dependent parameters, and these parameters can also be assumed to be the function of spatial coordinates and vary like other

parameters of FGM. However, for simplicity we have considered the fixed values of these parameters, i.e. the values of relaxation parameters are assumed as $t_1 = 0.15 \times 10^{-13}$s, $t_2 = 0.60 \times 10^{-14}$s.

Validation of the present method: The results computed by implementing the complete FEM and FEM with Newmark method are compared. It found that there is a perfect match in the results (see Fig. 3.5.1 and also Figs. 3.5.11-3.5.14), which validates the successful implementation of the present method. We further compare our results with the corresponding results obtained from a well established trans-finite element technique. The trans-finite element techniques employ an integral transform technique to eliminate time derivatives from the coupled equations. Then, the finite element method is applied to determine the solution in the transformed domain and further, the solution in the desired time domain is obtained by implementing a numerical inversion technique (see refs. Stehfest (1970); Bellman et. al. (1966), etc.). Here, the trans-finite technique is considered, which involves Laplace transform and numerical inversion of Laplace transform techniques. The details of this method can be found in the article by Bagri and Eslami (2008). For numerical inversion of Laplace transform, the Bellman method of Laplace inversion (Bellman et al. (1966)) is considered. A perfect match is observed in the solutions of all field variables obtained by all three methods (present method, FEM with Newmark method and trans-finite element). However, we display only the temperature distributions computed by all three methods and show the perfect match in the behaviour of the field variables which verify the present FEM formulations to be correct. Further, the computation time is calculated to run the MATLAB programs for each of the three methods for 4 different values of non-homogeneity index n. The bar plot (Fig. 3.5.2) showing the computation time taken by all three methods clearly indicates that the computation time of the present method is the same as FEM with Newmark method. However, it is much smaller as compared to the trans-FEM method and reflects the efficiency of the present complete finite element method over the trans-FEM method.

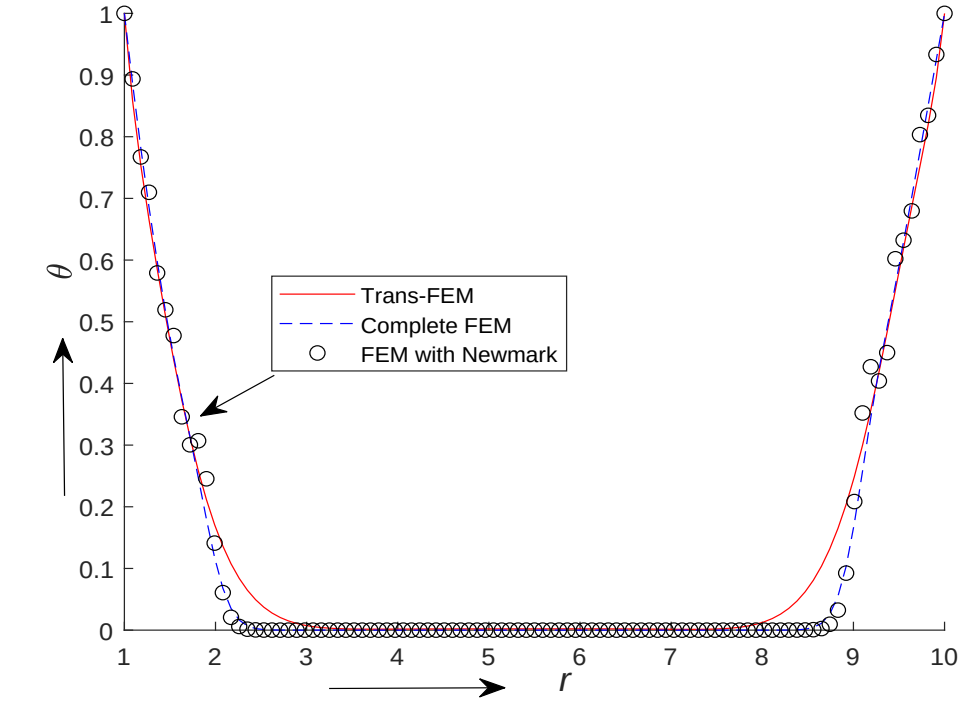

(a) $t = 0.40$

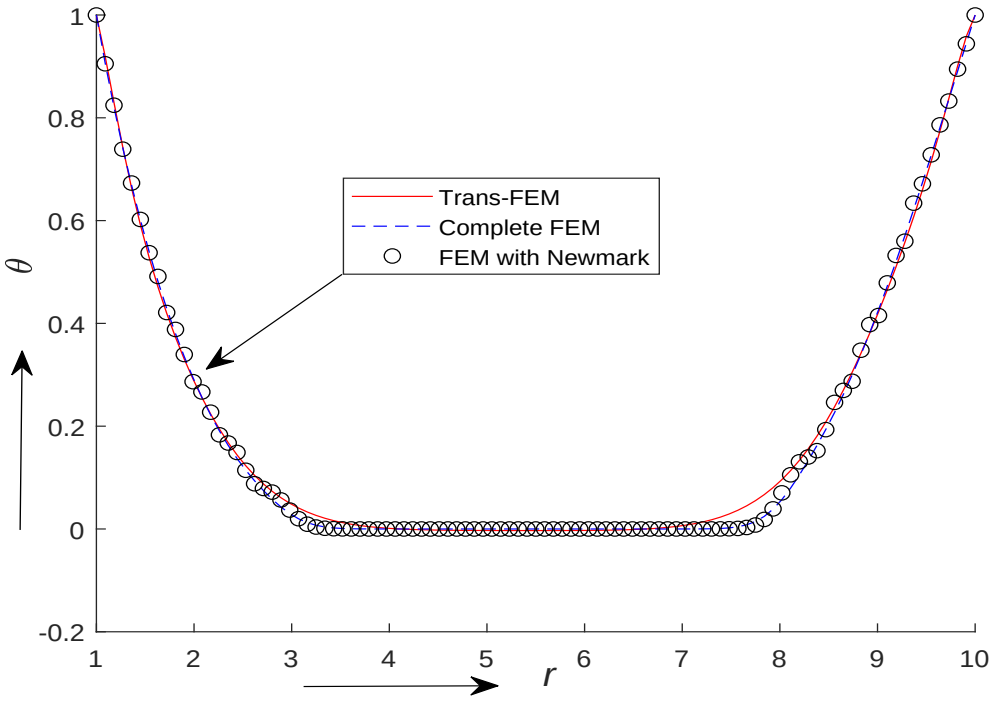

(b) $t = 0.69$

Figure 3.5.1: Temperature distribution at $t = 0.40$ and $t = 0.69$ under MGL theory for all methods

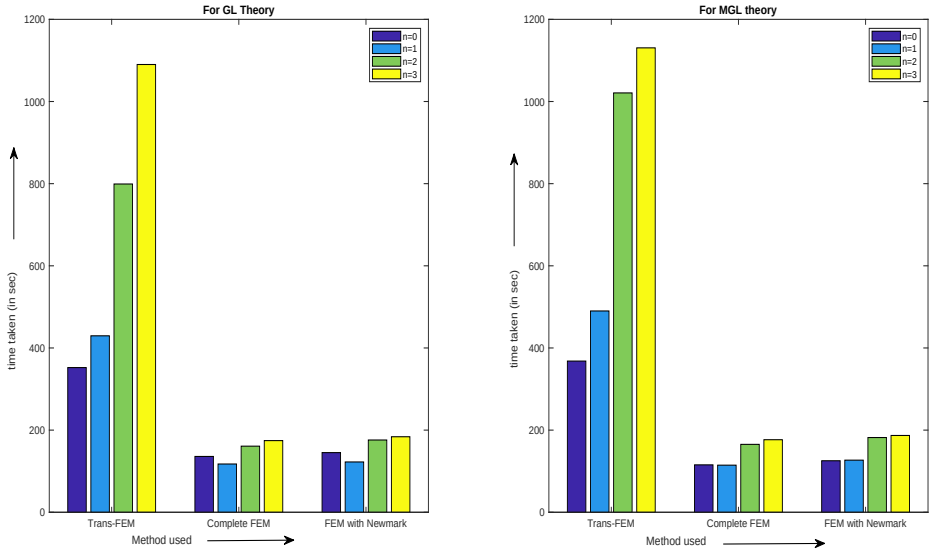

Figure 3.5.2: Comparison of CPU time for three different methods: Complete FEM, FEM with Newmark and Trans-FEM methods

Next, the results of the present problem predicted by the MGL model in various figures show the difference in results obtained by this theory with the corresponding results under GL theory. In order to show the effects of the non-homogeneity index on the behaviour of all field variables, the computation is carried out by taking various values of n. Here, the results obtained from the complete FEM approach are shown by 3D plots representing the space-time variations of all field variables for the cases when $n = 0$ and 2. The 3D Figs. 3.5.3-3.5.10 show the variation of the field variables with respect to space and time simultaneously in the context of the present (MGL) and GL model obtained by employing complete FEM. The behaviour of the field variables at any particular time can be observed closely from these 3D plots. Figs. 3.5.3 (a,b), 3.5.5 (a,b), 3.5.7 (a,b) and 3.5.9 (a,b) represent the variations of displacement, temperature, radial stress and circumferential stress, respectively, for GL theory and Figs. 3.5.4 (a,b). 3.5.6 (a,b), 3.5.8 (a,b) and 3.5.10 (a,b) are representing the variation of displacement, temperature, radial stress and circumferential stress, respectively, in the context of MGL theory for two different values of non-homogeneity index n.

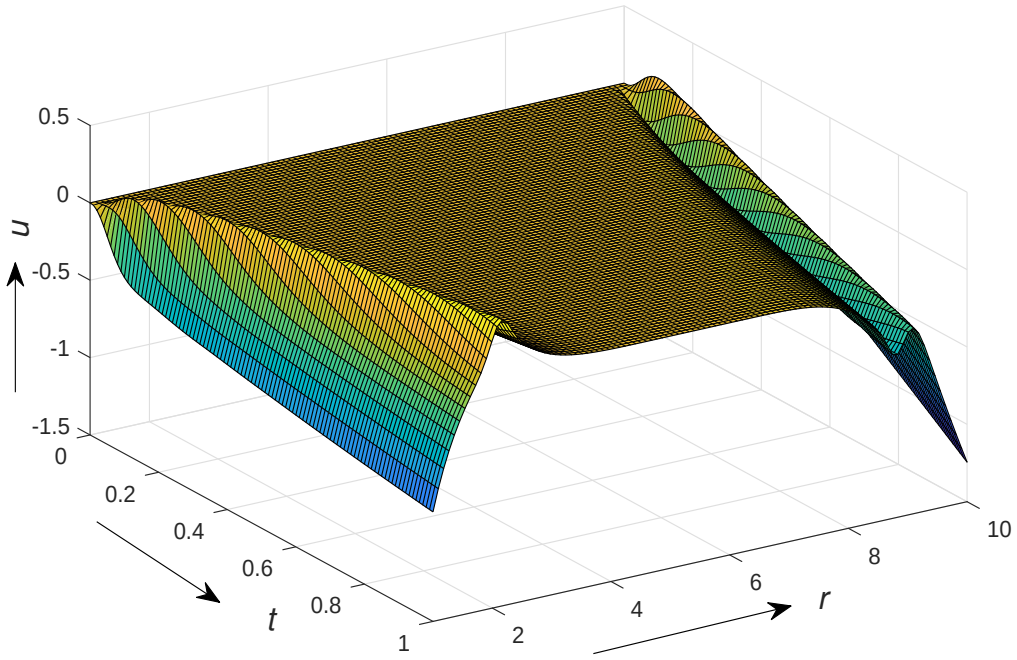

(a)

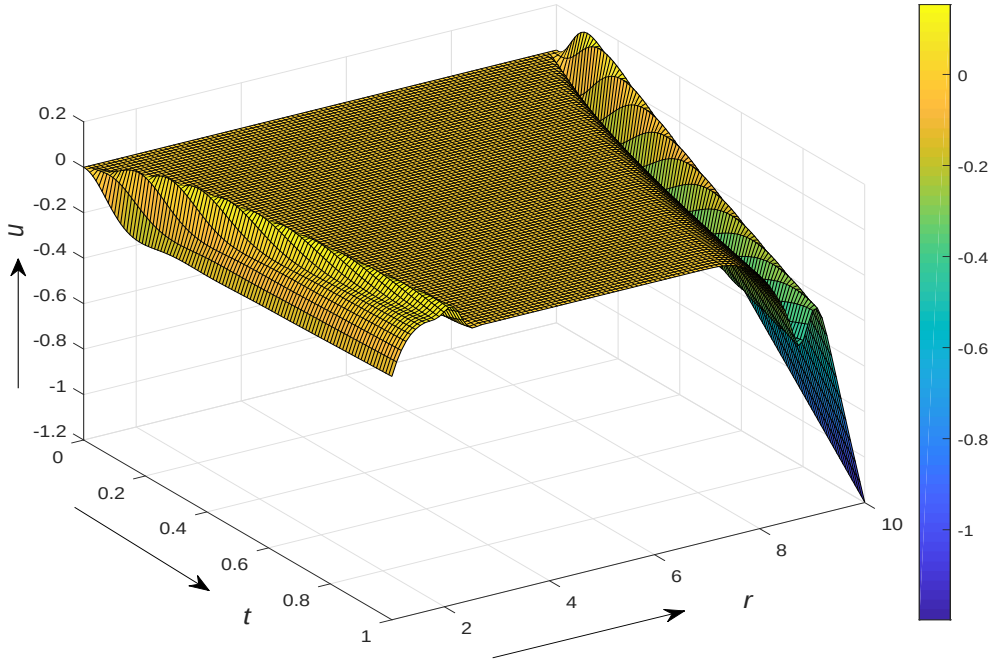

(b)

Figure 3.5.3: Variation of displacement (u) with r and t under GL theory for different n, (a) $n = 0$ and (b) $n = 2$

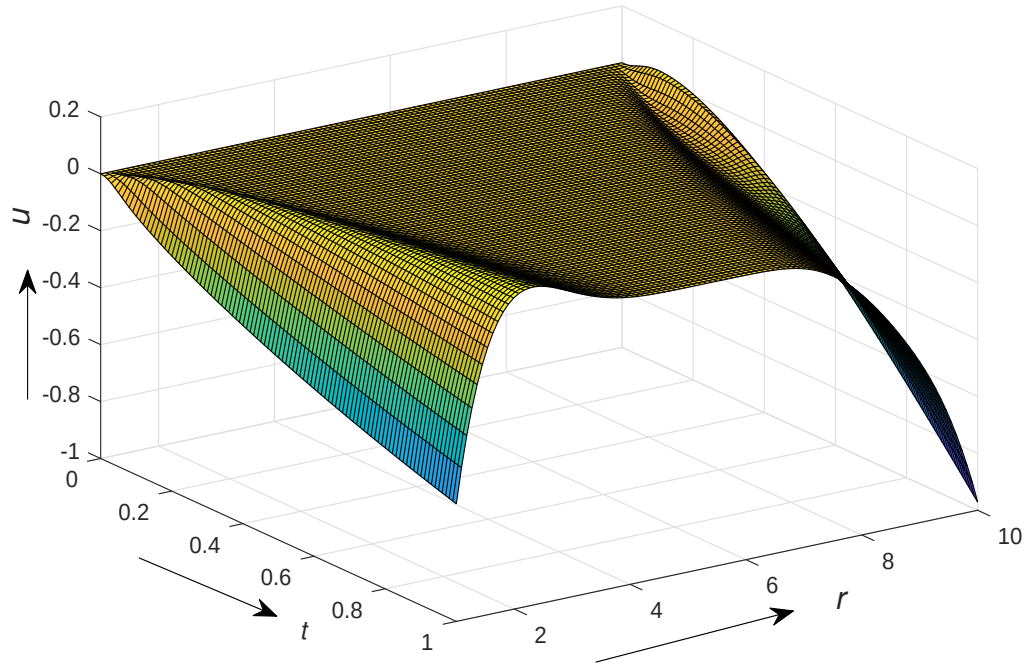

(a)

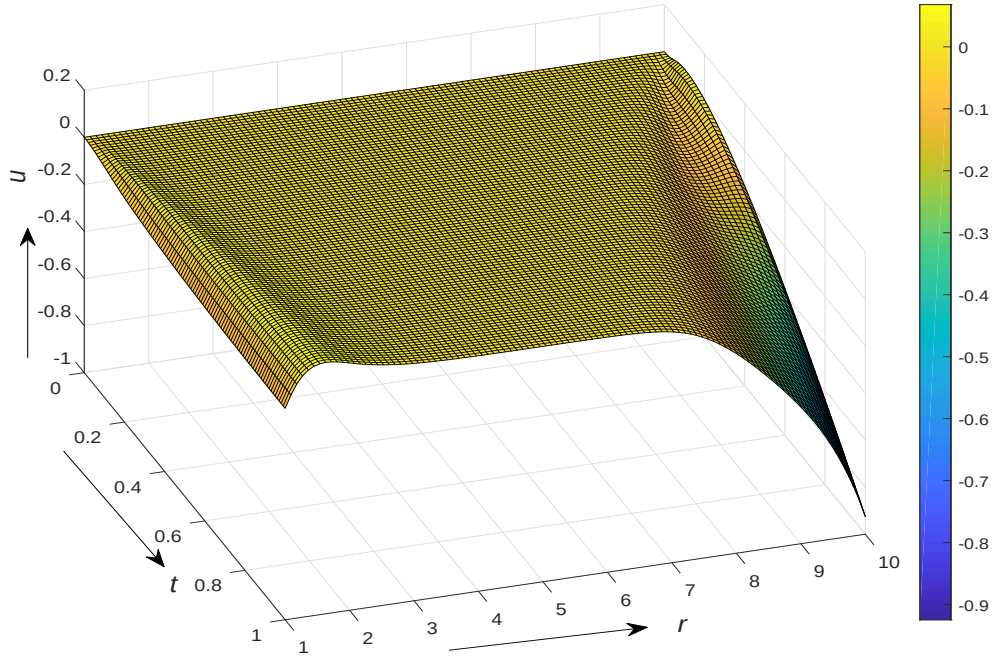

(b)

Figure 3.5.4: Variation of displacement (u) with r and t under MGL theory for different n, (a) $n = 0$ and (b) $n = 2$

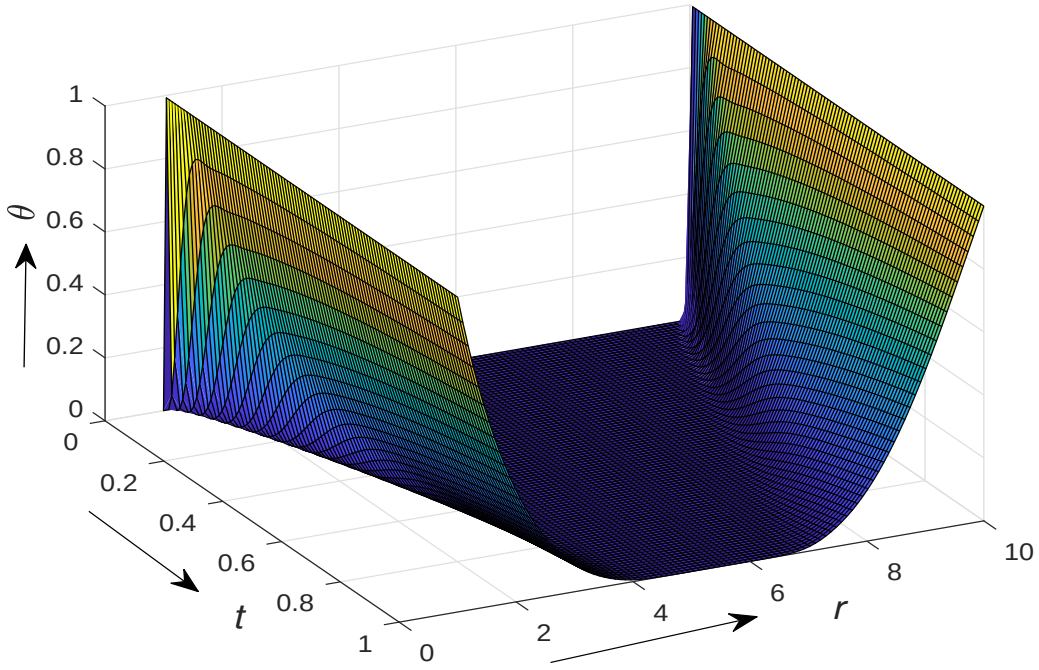

(a)

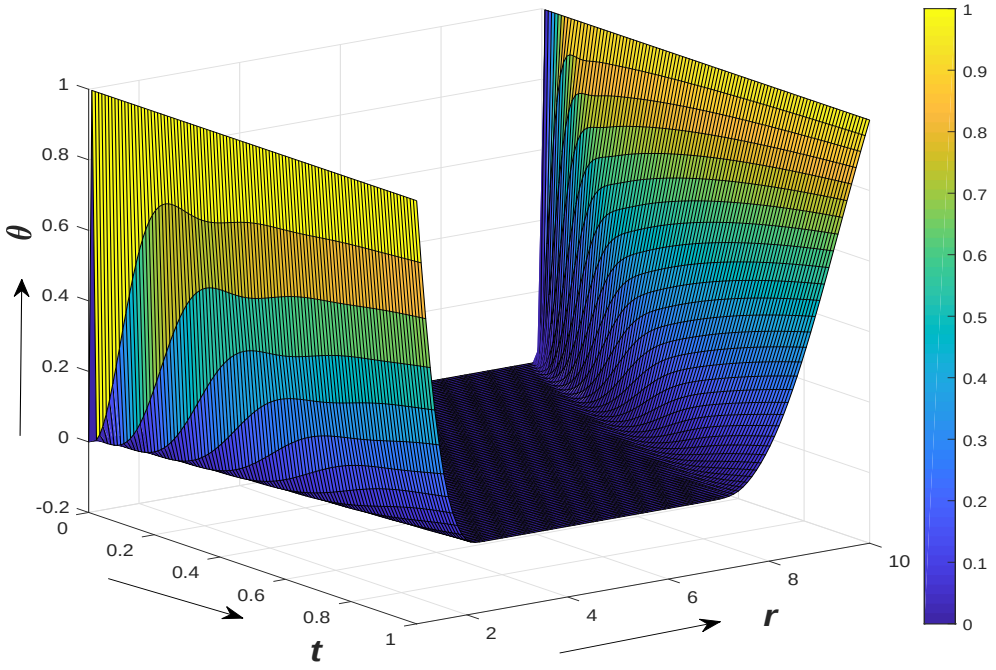

(b)

Figure 3.5.5: Variation of temperature (θ) with r and t under GL theory for different n, (a) $n = 0$ and (b) $n = 2$

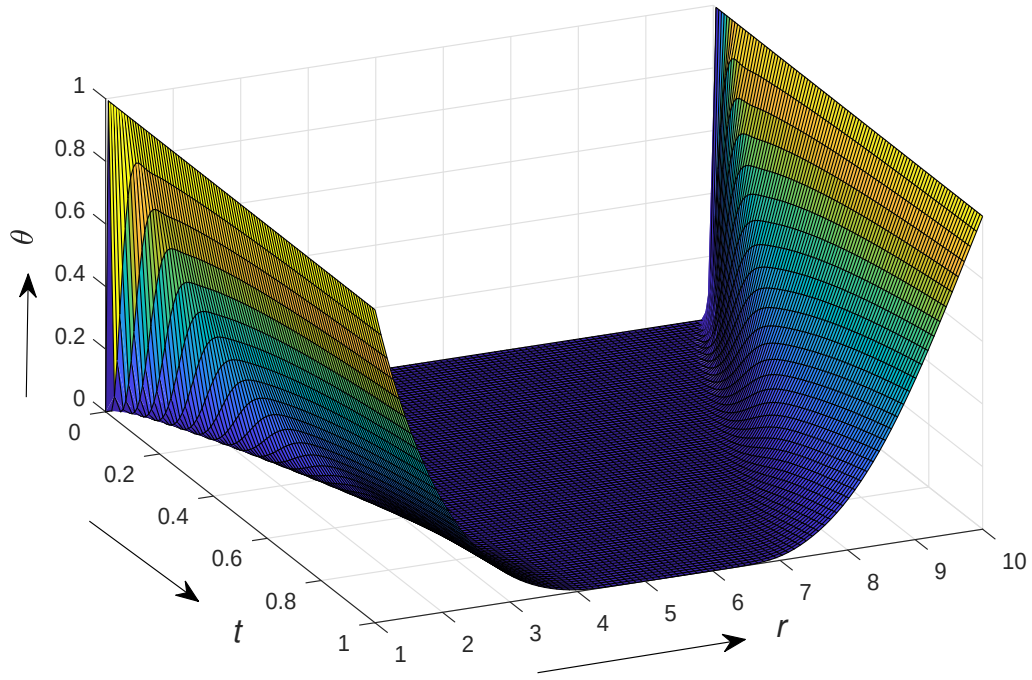

(a)

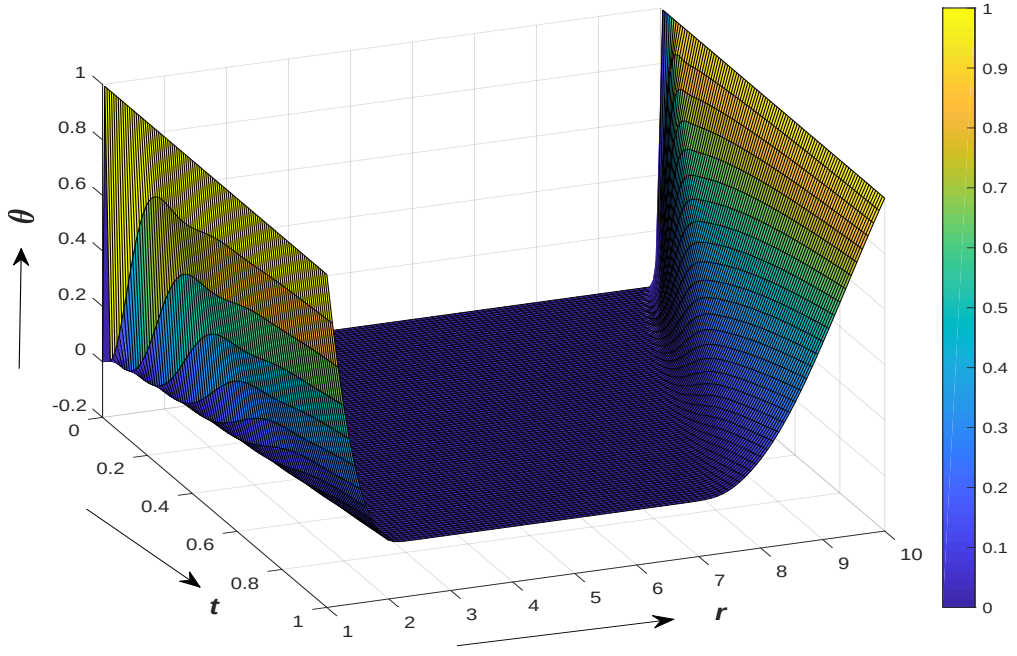

(b)

Figure 3.5.6: Variation of temperature (θ) with r and t under MGL theory for different n, (a) $n = 0$ and (b) $n = 2$

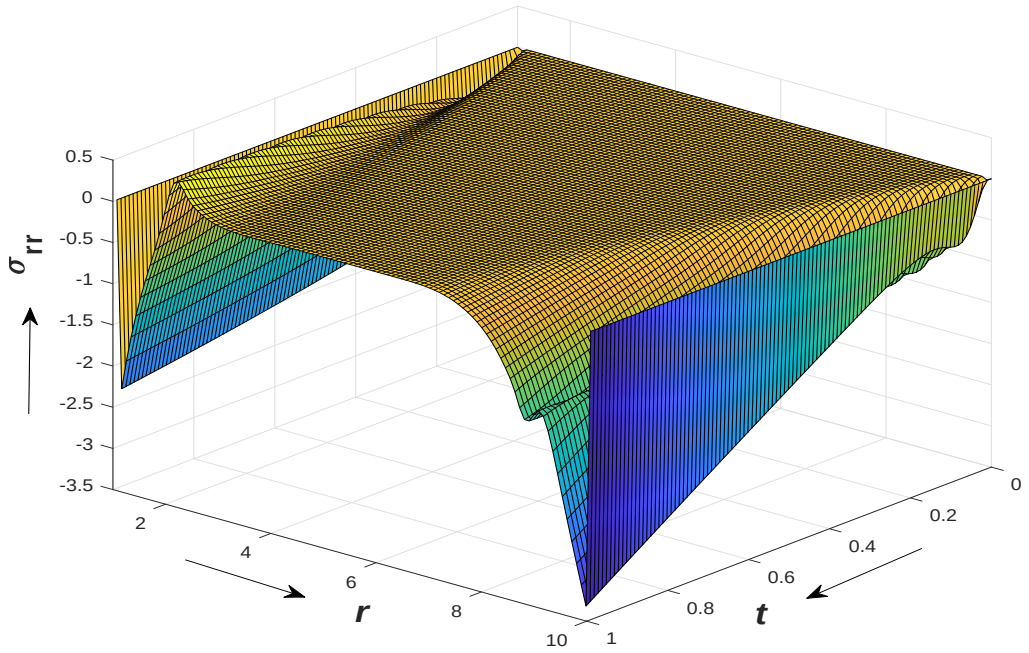

(a)

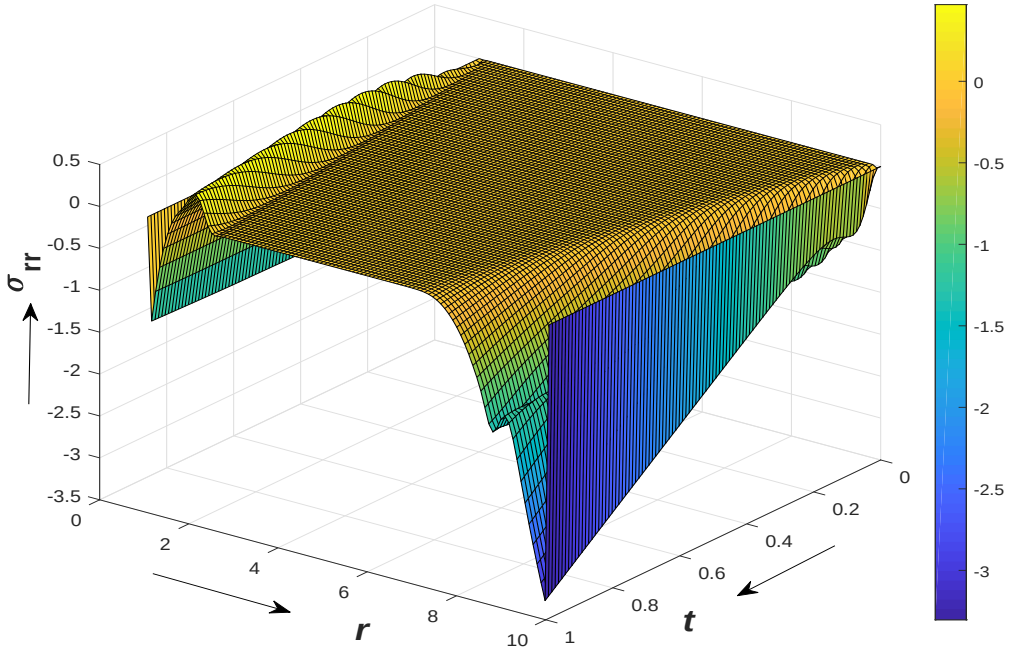

(b)

Figure 3.5.7: Variation of radial stress (σ_{rr}) with r and t under GL theory for different n, (a) $n = 0$ and (b) $n = 2$

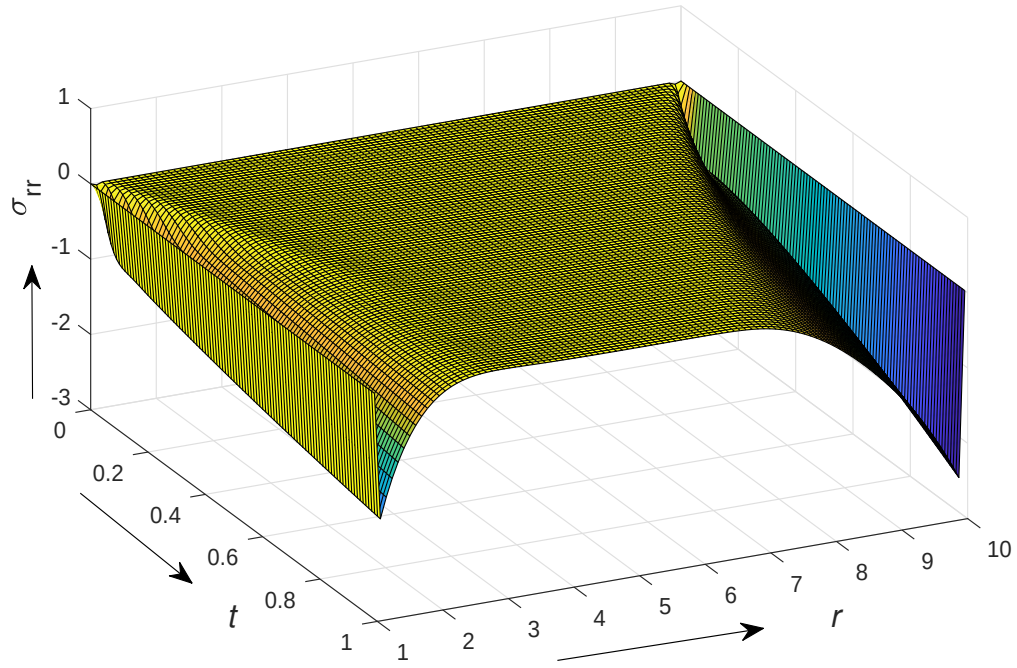

(a)

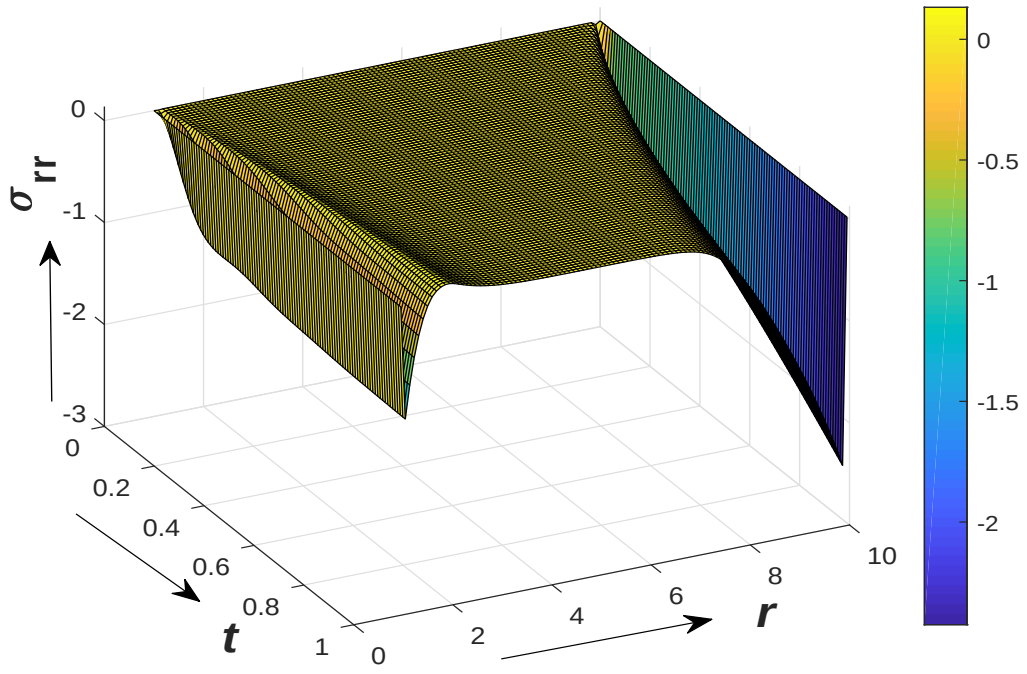

(b)

Figure 3.5.8: Variation of radial stress (σ_{rr}) with r and t under MGL theory for different n, (a) $n = 0$ and (b) $n = 2$

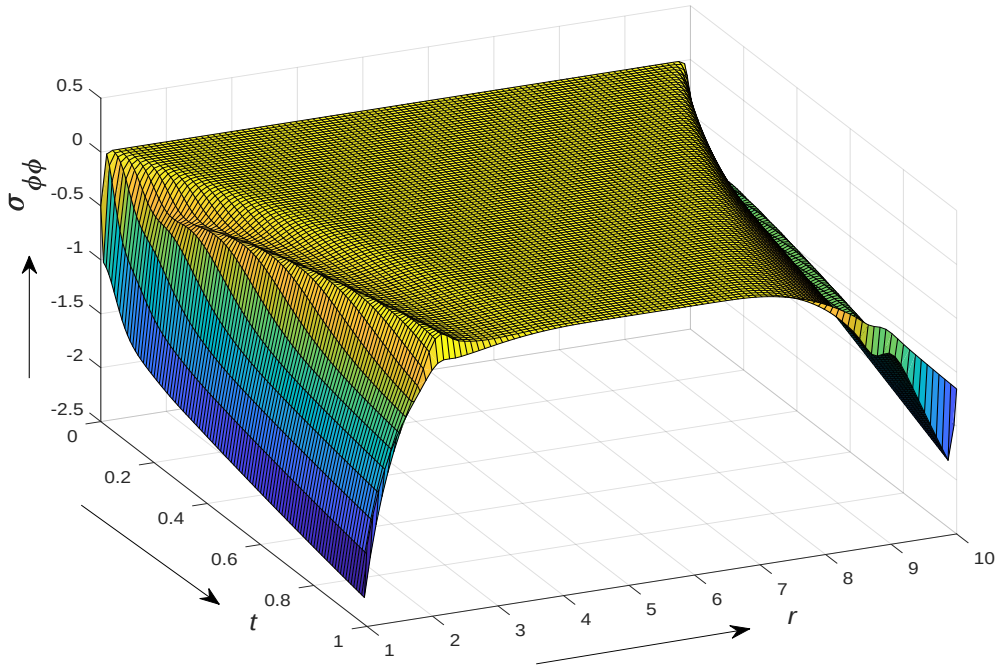

(a)

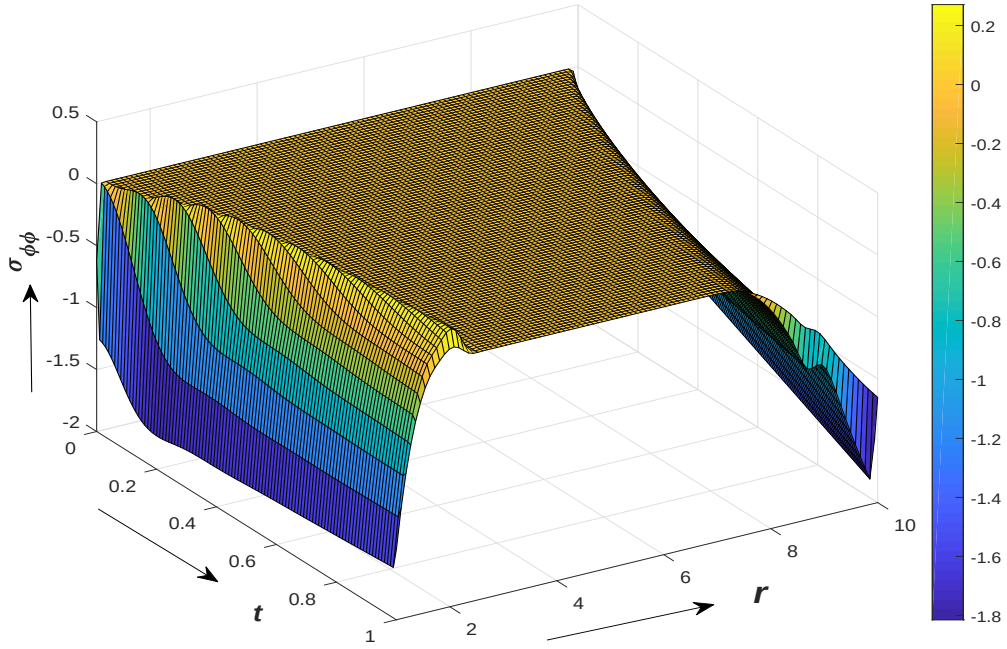

(b)

Figure 3.5.9: Variation of circumferential stress ($\sigma_{\phi\phi}$) with r and t under GL theory for different n, (a) $n = 0$ and (b) $n = 2$

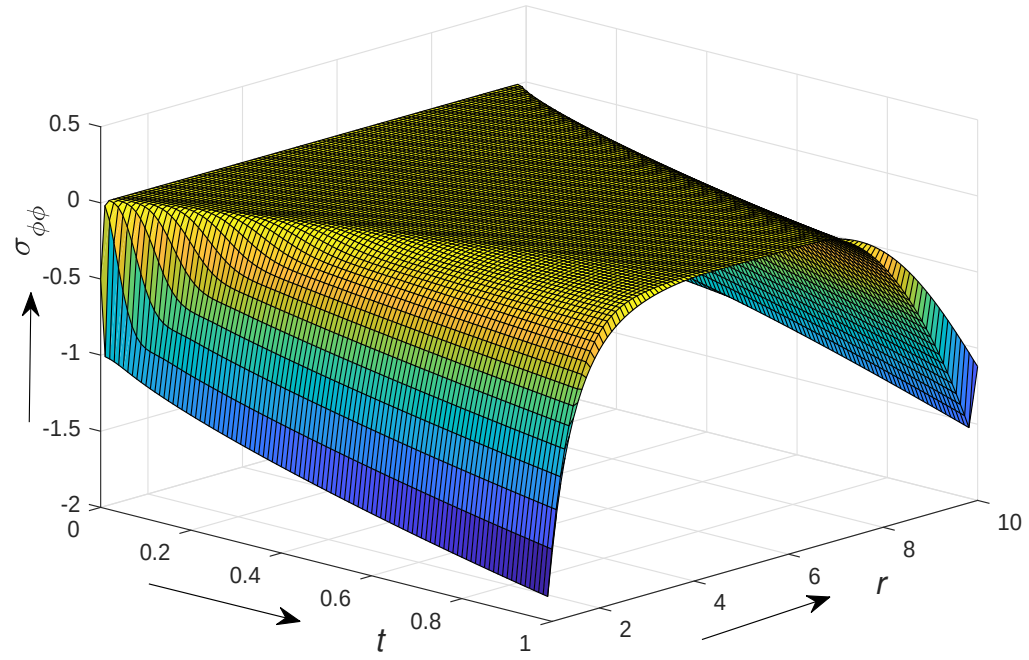

(a)

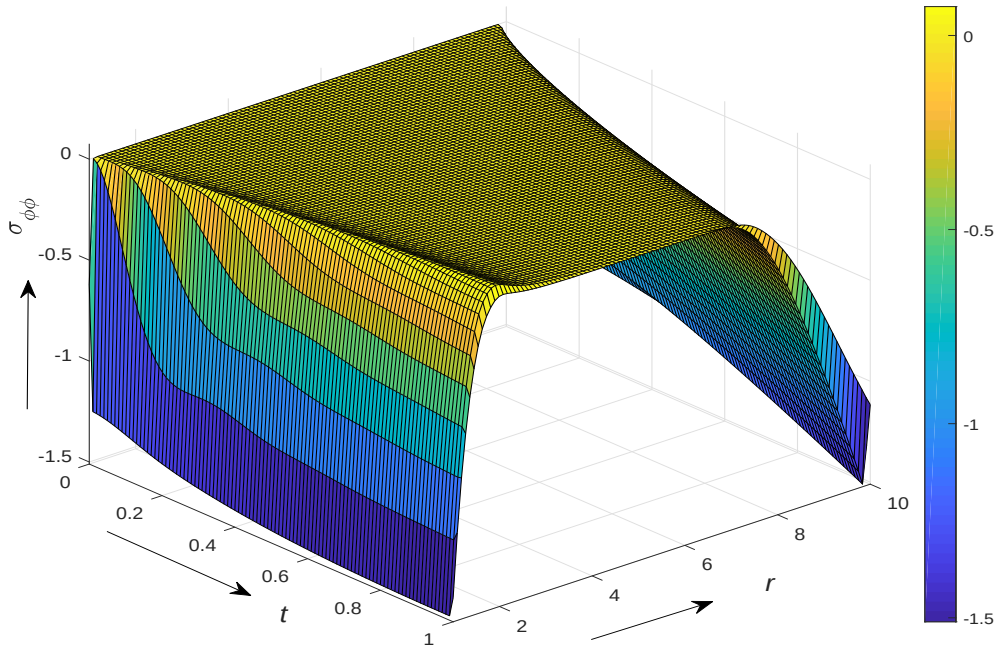

(b)

Figure 3.5.10: Variation of circumferential stress ($\sigma_{\phi\phi}$) with r and t under MGL for different n, (a) $n = 0$ and (b) $n = 2$

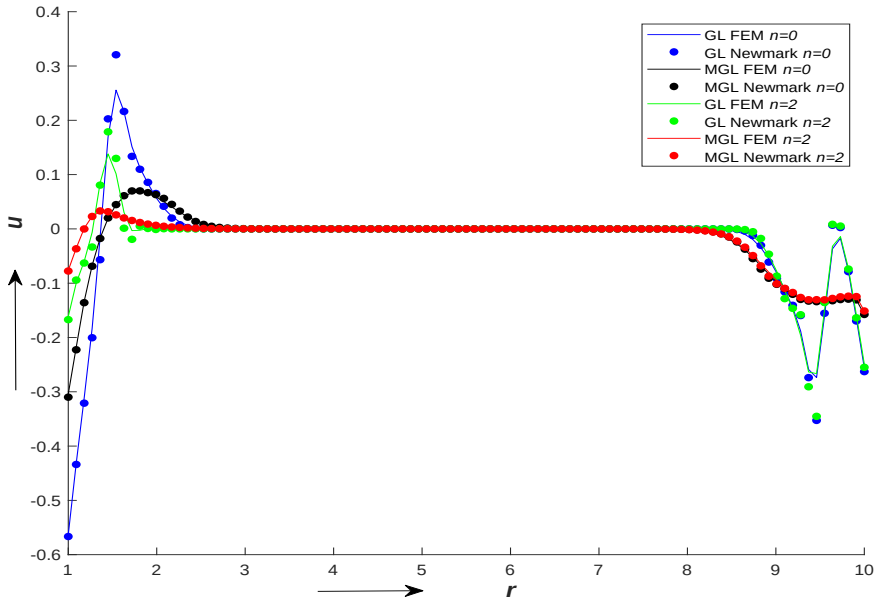

Figure 3.5.11: The effect of non-homogeneity on displacement (u) at $t = 0.40$ under GL and MGL model

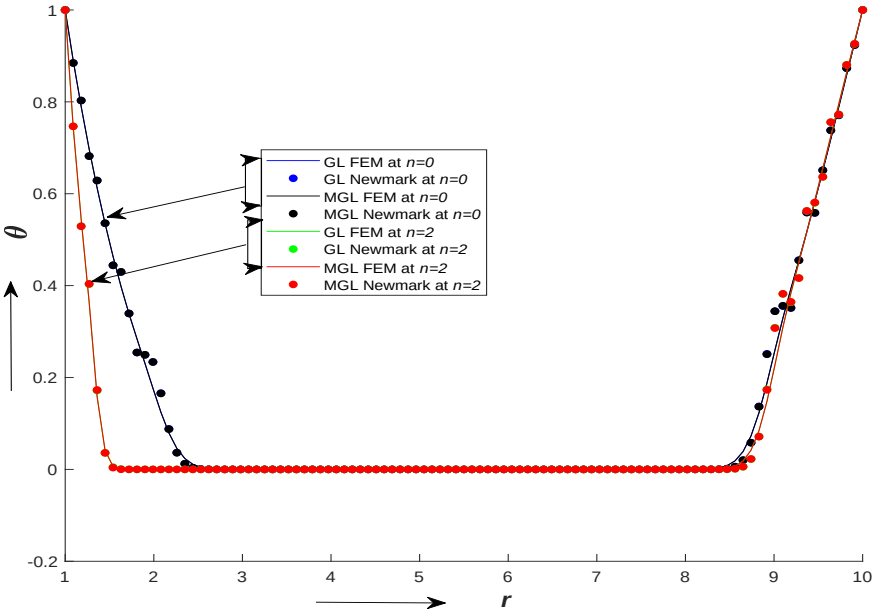

Figure 3.5.12: The effect of non-homogeneity on temperature (θ) at $t = 0.40$ under GL and MGL model

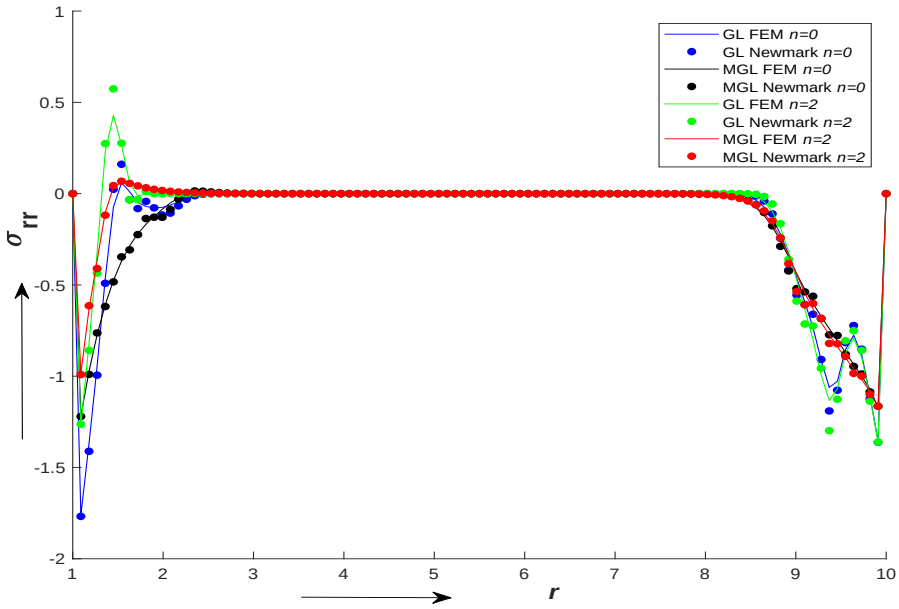

Figure 3.5.13: The effect of non-homogeneity on radial stress (σ_{rr}) at $t = 0.40$ under GL and MGL model

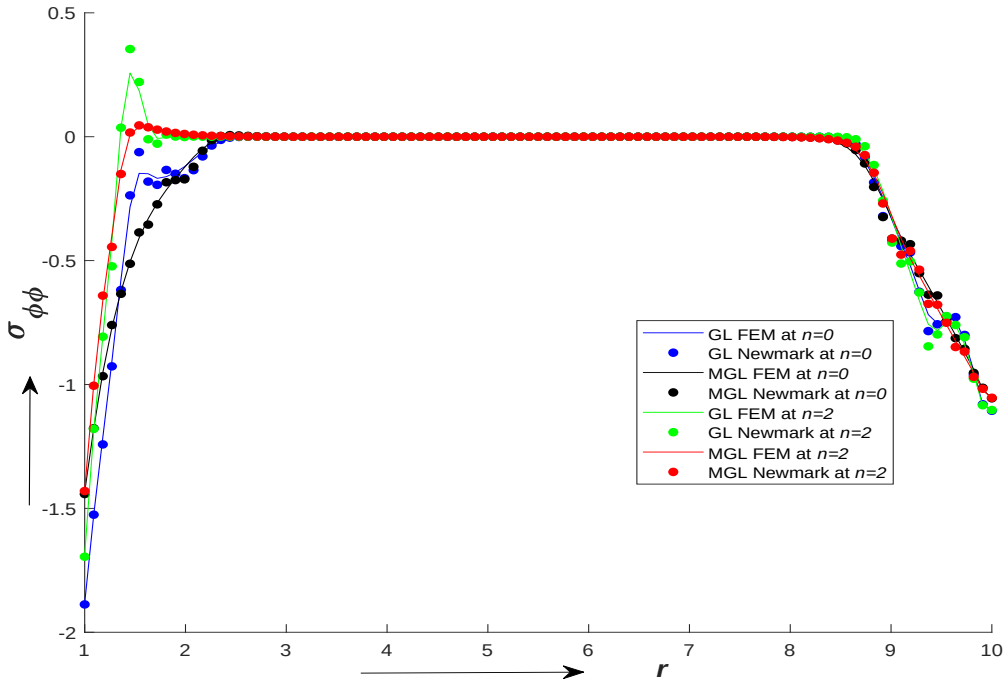

Figure 3.5.14: The effect of non-homogeneity on circumferential stress ($\sigma_{\phi\phi}$) at $t = 0.40$ under GL and MGL model

Figures 3.5.3-3.5.10 (a) are plotted to show the case when $n = 0$, i.e. material is entirely metallic and Figs. 3.5.3-3.5.10 (b) display the case when $n = 2$. Further, the line plots are used to compare the results obtained from the complete FEM approach and FEM with Newmark method. Figs. 3.5.11-3.5.14 show the line plots of different field variables along the radial direction at $t = 0.40$ for $n = 0$ and 2, under GL and MGL theories for both methods. A perfect match is observed in the solutions obtained by employing both approaches.

From the Figs. 3.5.3-3.5.10 (a,b) and Figs. 3.5.11-3.5.14, it is noticed that all field variables have the same pattern of behaviour for GL and MGL theories, and the results of the temperature field almost coincide for GL and MGL theories. However, a significant difference in predictions by GL and MGL theories can be seen for the displacement and both the stress components. The line plot shown in Fig. 3.5.11 yields that the displacement grows to higher values in the case of GL theory as compared to the case of MGL theory. However, the plots (Figs. 3.5.13-3.5.14) indicate that the radial and circumferential stresses for MGL theory attain a higher range of values in comparison to GL theory. The effective domain of influence in the case of MGL theory is much larger than the domain of influence under GL theory for all field variables, except the temperature field.

As the thermal shocks are applied on both the inner as well as outer boundaries of the disk, the behaviour of field variables are oscillatory in nature near the boundaries, and the differeneces in predictions by GL and MGL models are very much significant in this region. The effect of non-homogeneity index n is also prominent in the regions nearer to the boundaries. Here, the material of the disk is considered in such a way that its ceramic property is decreasing, and the metallic property is increasing radially from the inner boundary to the outer boundary. The prominent effect of n is observed in the region nearer to inner boundary, i.e., for FGMs with more ceramic component, and it is more significant for stress fields.

At the initial time of interaction, the effect can be visible only in the region nearer to the boundaries. However, as time increases, the effect can be observed on the larger domain, implying that the effective domain of influence increases with the increase of time. The disagreement of the two theories also increases at the higher time of thermomechanical interactions.

The effect of the non-homogeneity index, n is significant under both GL and MGL models. Figs. 3.5.3-3.5.14 indicate that the effective domain decreases as we increase the values of n. Moreover, the effect of the non-homogeneity index is most significant in the context of the MGL theory as compared to GL theory.

3.6 Conclusion

The present work is concerned with the mathematical modeling for a coupled problem of thermoelasticity for a functionally graded hollow disk under strain and temperature-rate dependent theory by applying a complete Galerkin's approach for both space and time. The unified equations for the temperature-rate (GL), as well as strain and temperature-rate (MGL) dependent theories, are derived, and a complete Galerkin's finite element method is applied to obtain the finite element equations of the space domain, and then we have implemented a FE approach as an alternative to the Newmark method. Galerkin's approach is employed to derive the explicit iterative scheme to obtain the final solution in the space-time domain. Next, for the validation of the method, the Newmark time integration scheme is applied for solving the time differential system of equations. From the line plots field variables, it is shown that the results obtained by our method match completely with the results by FEM with Newmark method.

A detailed analysis of our results highlights the effects of non-homogeneity of material properties on the variations of different field variables for GL and MGL theories. A significant difference in the predictions by MGL theory as compared to the predictions

by GL theory is observed. It is investigated that all the variables finally tend to zero values after some distance from the inner and outer boundaries, which is the source of thermomechanical interactions inside the hollow disk. The effective domain increases with the increase in time and decreases with the increase in the non-homogeneity index. The stress fields are noted to be largely affected due to functionally graded material properties. Further, the MGL model indicates a larger effective domain. The validation of the present formulation is also confirmed by comparing the present results with the corresponding results obtained by employing trans-FEM. The present method is found to be more efficient like FEM with Newmark method as compared to trans-FEM, since it lowers calculation time by at least 3-4 times. Hence, the method based on the complete FEM approach is assumed to be an efficient method for solving the dynamical problems of coupled thermoelasticity for homogeneous or non-homogeneous mediums.